Electronic Supplementary Material (ESI) for Journal of Materials Chemistry C.

Supplementary information

Highly Efficient Bilateral Doping of Single-Walled Carbon Nanotubes

Anastasia E. Goldt[a], *Orysia T. Zaremba*[a], *Mikhail O. Bulavskiy*[a], *Fedor S. Fedorov*[a],

Konstantin V. Larionov[b,c], *Alexey P. Tsapenko*[d], *Zakhar I. Popov*[b,e], *Pavel Sorokin*[b],

Anton S. Anisimov[f], *Heena Inani*[g], *Jani Kotakoski*[g], *Kimmo Mustonen*[g], *Albert G. Nasibulin*[a,h]*

[a]Skolkovo Institute of Science and Technology, 3 Nobel Street, 121205 Moscow, Russia

[b] National University of Science and Technology "MISiS", Leninsky prospect 4, 119049 Moscow, Russian Federation

[c]Moscow Institute of Physics and Technology, Institutskiy lane 9, Dolgoprudny, 141700 Moscow region, Russian Federation

[d]Aalto University, Department of Applied Physics, Puumiehenkuja 2, 00076 Espoo, Finland

[e]Emanuel Institute of Biochemical Physics RAS, 119334 Moscow, Russian Federation

[f]Canatu Ltd., Konalankuja 5, 00390 Helsinki, Finland

[g]Faculty of Physics, University of Vienna, Boltzmanngasse 5, 1090 Vienna, Austria

[h]Aalto University School of Chemical Engineering, Kemistintie 1, 16100 Espoo, Finland

1. Thermal Treatment Optimization

To optimize our method for efficient SWCNT doping utilizing their inner space for dopant incorporation, we evaluated optoelectronic and structural changes, induced by SWCNT thermal treatment in the range of 100 – 500 ˚C. For these purposes, we used UV-vis-NIR and Raman spectroscopies, TEM imaging, and four-probe sheet resistance measurements.

1.1. Changes in Optical and Electrical Properties Induced by Thermal Treatment

UV-vis-NIR absorption spectra were measured to analyze the electronic states of SWCNTs before and after the thermal treatment (Figure S1a). Spectra usually clearly display the excitonic transitions between van Hove singularities in semiconducting (E_{11} and E_{22}) and metallic (M_{11}) SWCNTs. It should be noted that SWCNT films are environmentally doped by adsorbed gaseous species. In order to clearly represent the processes occurring during the thermal treatment in the temperature range examined, we plotted the absorbance values at the wavelengths of 2378, 1310, and 894 nm, which corresponded to the mean value of E_{11}, $E_{22,}$ and M_{11} transitions (Figure S1b). S_{11} peak intensity exhibits significant monotonous growth with the temperature increase up to 350 ˚C, the intensity of S_{22} peak is characterized by the same behavior pattern, although with a smaller growth rate, and the M_{11} peak remains nearly unaltered up to 350 ˚C. When the treatment temperatures surpass 350 ˚C, all peaks start to decrease remarkably. The initial growth of S_{11} and S_{22} peak intensities with temperature up to 350 ˚C can be attributed to the desorption of oxygen, which is known to be adsorbed on the SWCNT surface from the air leading to the *p*-doping effect.[S1] Rapid drop of all peak intensities at higher temperatures (400 ˚C and above) indicates the oxidation of SWCNTs, which starts from end-caps since they are the most reactive parts of nanotubes.[S2]

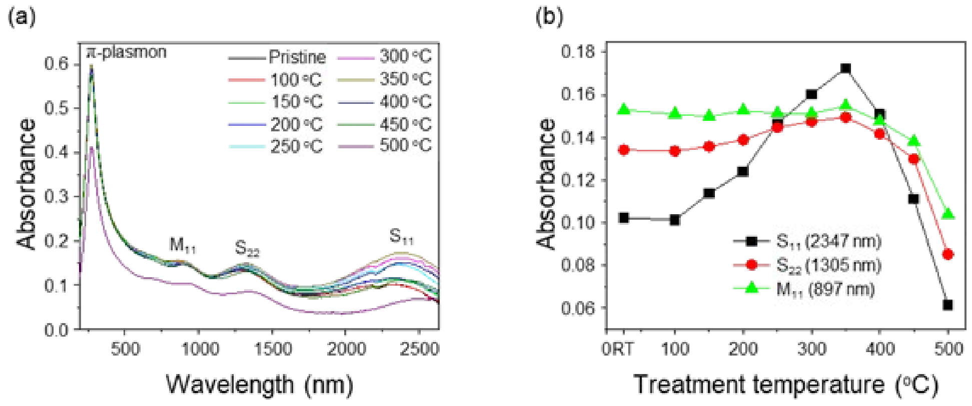

Fig. S1 UV-vis-NIR absorption spectra of the SWCNT films treated at different temperatures (a). S_{11} (2378 nm), S_{22} (1310 nm), and M_{11} (894 nm) peaks as a function of the treatment temperature (b).

Since transmittance (*T*) and equivalent sheet resistance (R_{90}) are quality defining parameters for transparent conductors, we monitored their variations with the change in the treatment temperature. Figure S2 represents relative changes in *T* and R_{90} in comparison to the pristine sample, as functions of the treatment temperature. Equivalent sheet resistance was calculated as:

$$R_{90} = R_s \cdot \frac{A}{\log_{10}\left(\frac{10}{9}\right)}, \tag{1}$$

where A and R_s are the absorbance (at 550 nm) and sheet resistance of the films.[S3]

The transmittance (Figure S2) remains almost unchanged when SWCNT films are treated at temperatures up to 350 ˚C, although at higher temperatures the transmittance increases markedly. The equivalent sheet resistance exhibits continuous growth with the increase of the treatment temperature, which can be explained by the desorption of oxygen from the SWCNT surface and the oxidation of SWCNTs at temperatures higher than 350 ˚C.

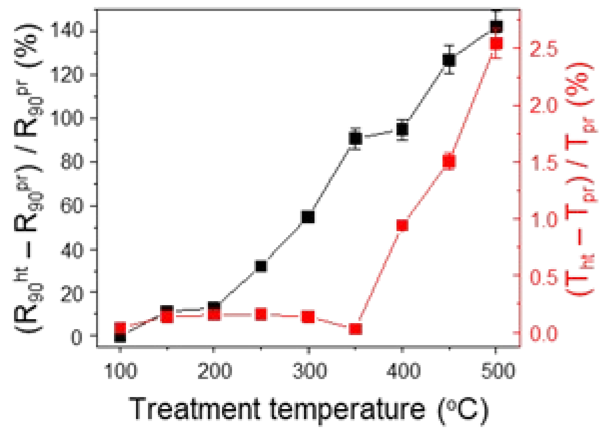

Fig. S2 Relative changes of transmittance and equivalent sheet resistance of SWCNT films *versus* the treatment temperature, ht signifies heat treated.

1.2. Structural Changes Caused by Thermal Treatment

The quality of SWCNTs was estimated as the ratio of intensities I_G/I_D calculated using Raman spectroscopy data. The thermal treatment of the SWCNT films up to 300 ˚C did not lead to significant changes in the I_G/I_D ratio. Further increase in the temperature caused a slight decrease in the I_G/I_D ratio, which might be attributed to the introduction of defects in the SWCNTs due to the oxidation process in the air (Figure S3a). These results are in accordance with the changes in the intensity distribution in the RBM frequency range with increasing treatment temperature (Figure S3a). The RBM peaks remain unaltered up to 300 ˚C, and a further increase in the temperature leads to the disappearance of RBM peaks corresponding to smaller diameters, which are more reactive.[S4]

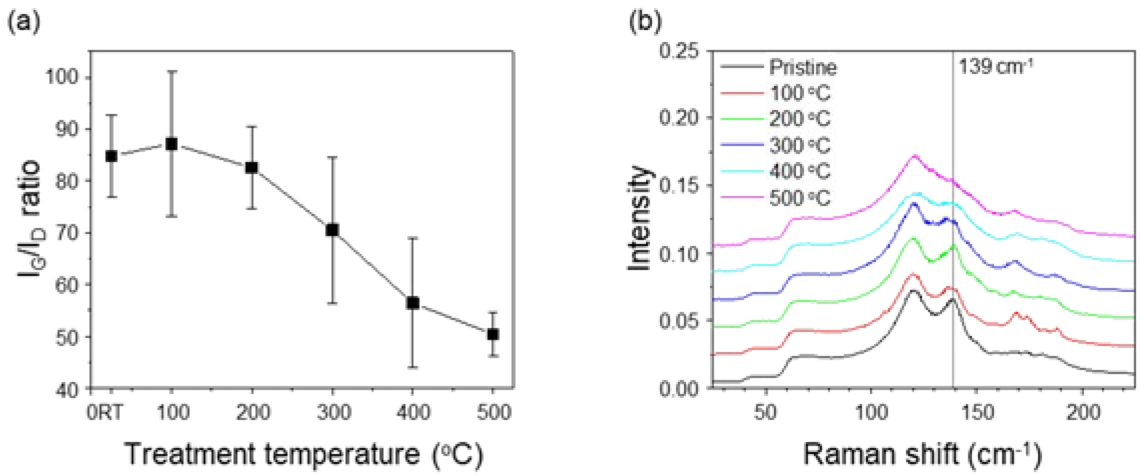

Fig. S3 Raman spectra alterations with thermal treatment of SWCNT films at different temperatures. Evolution of the I_G/I_D intensity ratio (a) and RBM-mode after treatment at different temperatures (b).

Figure S4 shows the typical TEM images of pristine SWCNT films and thermally treated at 300 and 400 °C . The morphology of the SWCNTs after the thermal treatment remained similar when compared to the pristine SWCNTs. We have plotted the diameter of bundles diameter, and it follows the Gaussian distribution. The calculation of mean diameters of bundles at different temperatures revealed that thermal treatment above 300 ˚C leads to a small increase in the average thickness of bundles from 7 (300 ˚C) to 10 (400 ˚C) nm due to an increase in the thermal energy during the treatment process.

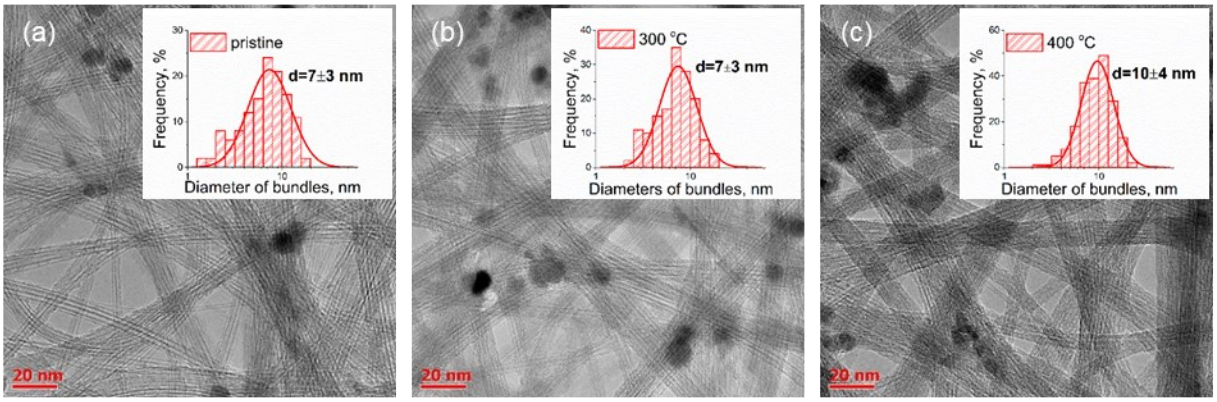

Fig. S4 Transmission electron microscopy images of SWCNTs films and corresponding bundle diameter distributions (insets) for the pristine film (a), after thermal treatment at 300 ˚C (b) and 400 ˚C (c).

2. $HAuCl_4$ Doping after Thermal Treatment of SWCNTs

To investigate the efficiency of the doping effect after thermal treatment and the formation of gold nanowires in the inner space of SWCNTs, we used Raman and XPS spectroscopies, STEM imaging, OCP measurements, and band structure calculations.

2.1. Raman Measurements of Doped SWCNTs

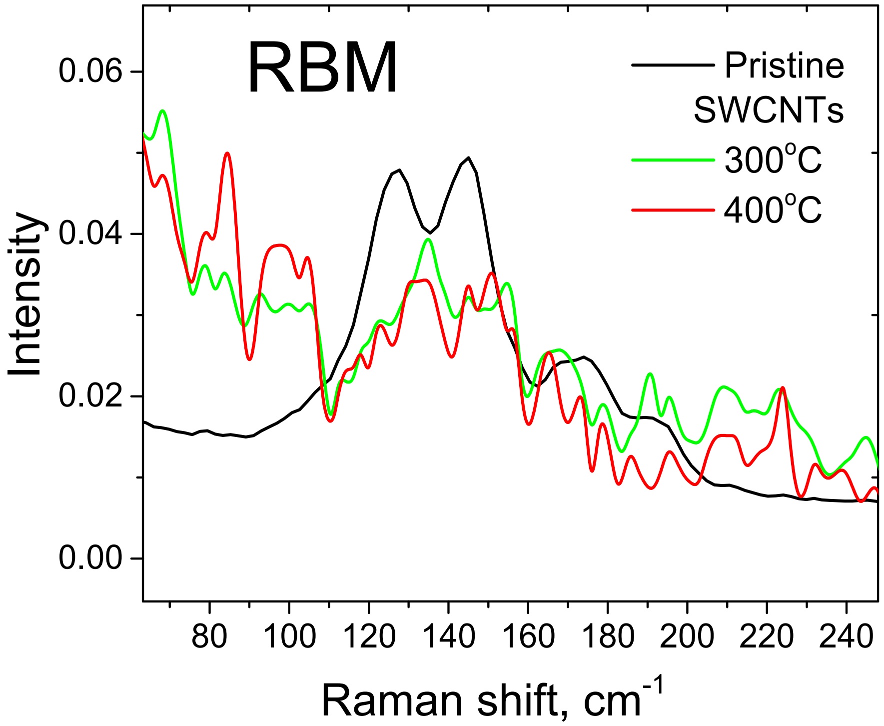

Fig. S5 RBM Raman spectra of $HAuCl_4$-doped SWCNTs: pristine and after thermal treatment at 300 and 400 °C.

2.2. STEM Measurements of Doped SWCNTs

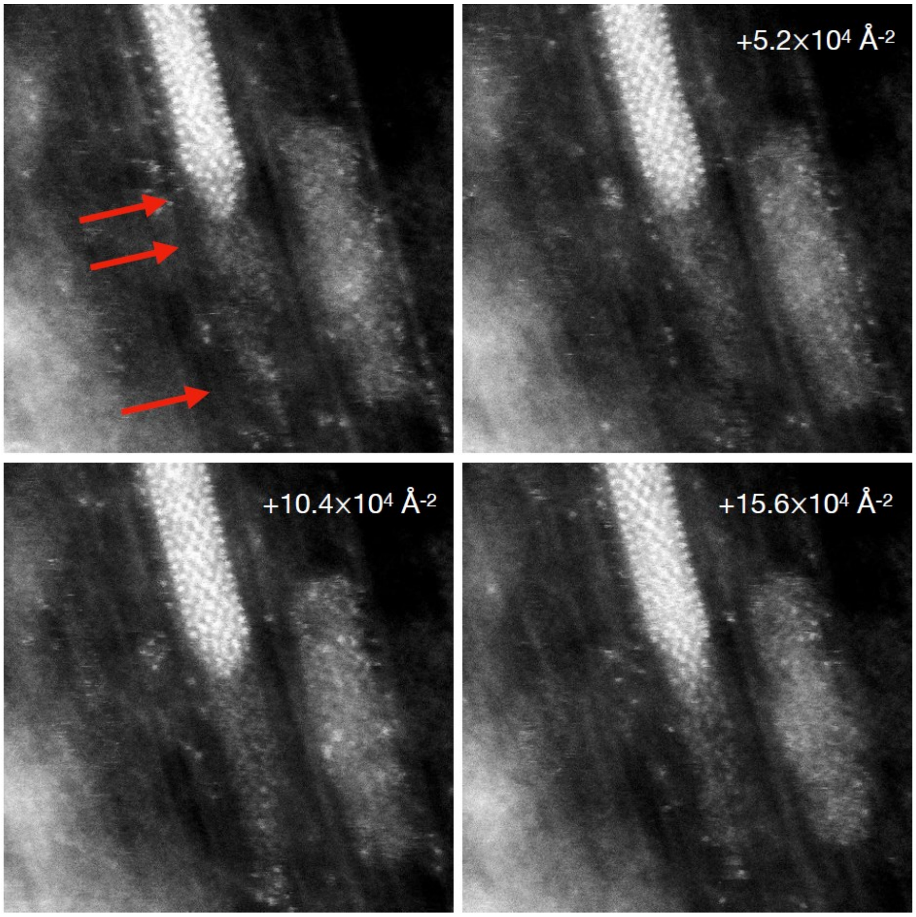

Fig. S6 *In situ* diffusion of gold along the nanotube axis, the position pointed out by the arrows (see also video). The diffusion process is driven by the scanning electron probe, the dose equivalent per each acquired frame is 5.2 x 10^4 $e^-/Å^2$ at 25 pA probe current.

2.3. OCP Measurement of Doped SWCNTs with and without Thermal Treatment

Figure S7 shows the OCP transient curves recorded for all probed SWCNT films: pristine (Figure S7a) and treated at 350 ˚C (Figure S7b) SWCNT films, immersed into $HAuCl_4$ ethanol solutions of concentrations varied from 7.5 to 60 mM.

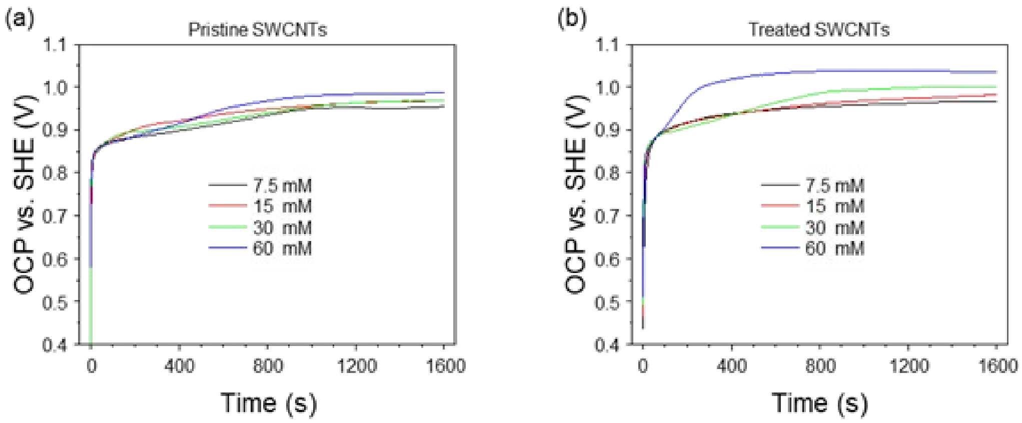

Fig. S7 OCP transient for pristine (a) and thermally treated SWCNTs (b) recorded in solutions of 7.5, 15, 30 and 60 mM $HAuCl_4$ concentrations.

2.4. XPS Measurements of Doped SWCNTs

The high-resolution XPS spectra of Au 4f and Cl 2p of 15 mM $HAuCl_4$-doped SWCNTs are depicted in Figure S8. By deconvolving the asymmetric Au 4f doublets, we can observe four components such as the reduced Au^0 clusters (Au^0 $4f_{5/2}$ and Au^0 $4f_{7/2}$) and the Au^{3+} ions (Au^{3+} $4f_{5/2}$ and Au^{3+} $4f_{7/2}$), as shown in Figure S8a. The higher peaks of Au^{3+} indicate the substantial amount of Au^{3+} that remains on nanotubes. This is confirmed by the Cl 2p core peak, which is attributed to metal chloride (Figure S8b).

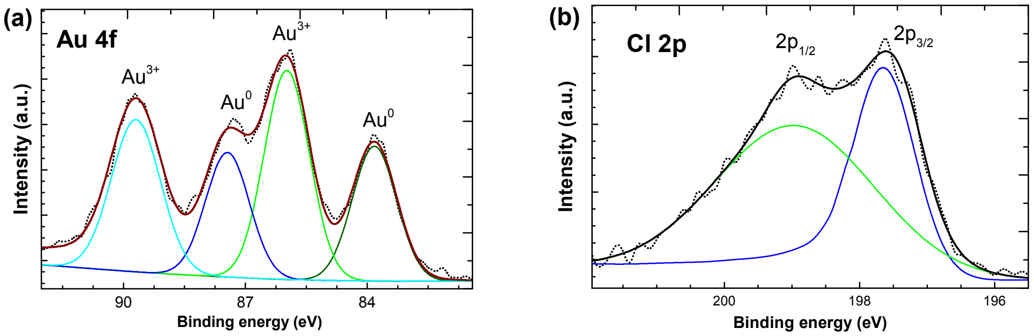

Fig. S8 XPS analysis of fitted (a) Au 4f and (b) Cl 2p core peaks.

2.5. Electronic Properties Calculations

Figure S9 shows band structures corresponding to pristine SWCNT (10,10), the same tube doped with $AuCl_4$ from the outside, and several additionally doped SWCNTs from the inside with different $AuCl_x$ dopants.

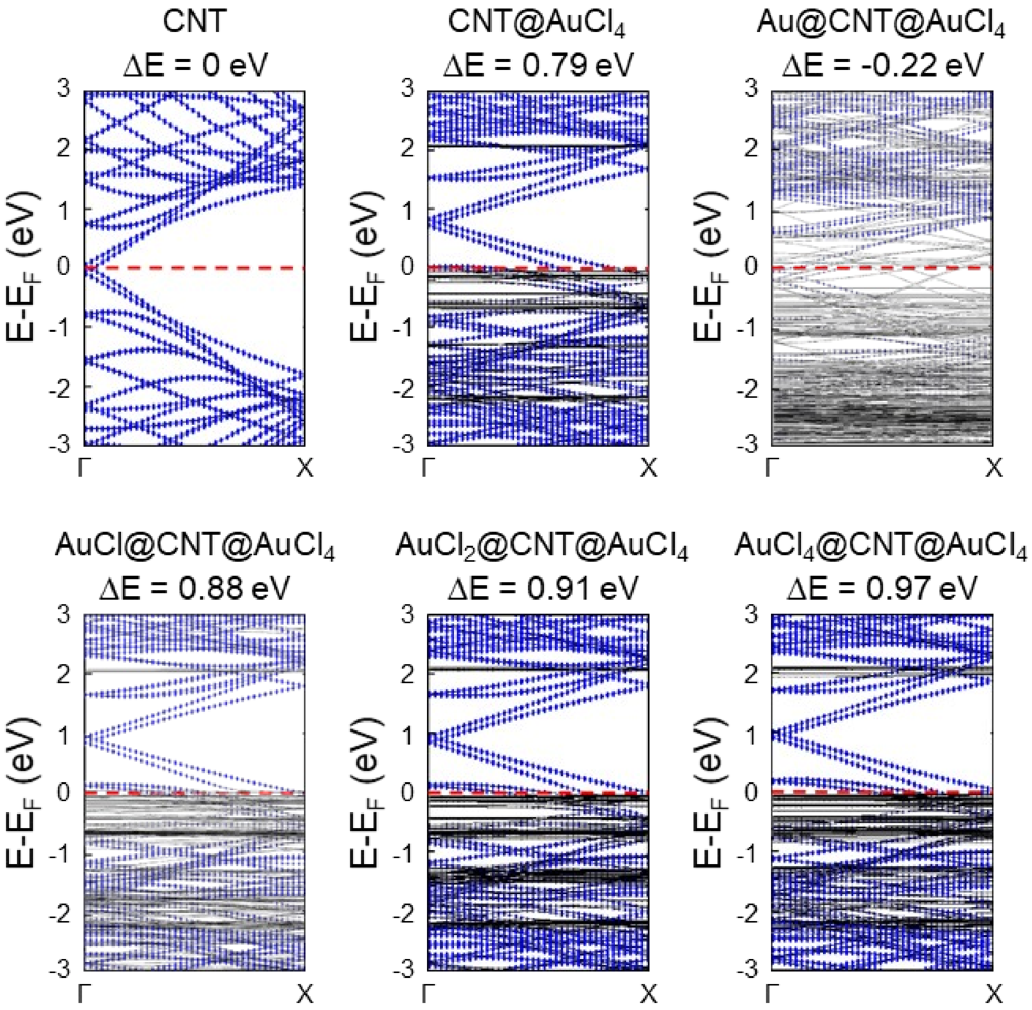

Fig. S9 Band structures of pristine SWCNT (10,10), doped with $AuCl_4$ from the outside, and doped from both the inside and outside with different $AuCl_x$ dopants as shown in Figure 5. Fermi level is indicated with a red dashed line, the blue dots correspond to contributions from carbon atoms.

References:

S1. S. D. Shandakov, M. V. Lomakin, A. G. Nasibulin, *Tech. Phys. Lett.* 2016, **42**, 1071–1075.

S2. X. Yu, J. Zhang, W. Choi, J. Y. Choi, J. M. Kim, L. Gan, Z. Liu, *Nano Lett.* 2010, **10**, 3343–3349.

S3. I. V. Anoshkin, A.G. Nasibulin, Y. Tian, B. Liu, H. Jiang, E.I. Kauppinen, *Carbon,* 2014, **78**, 130–136.

S4. B. Liu, H. Jiang, A.V. Krasheninnikov, A.G. Nasibulin, W. Ren, C. Liu, E.I. Kauppinen, H.M. Cheng, *Small,* 2013, **9**, 1379–1386.